MSDM: GENERATING TASK-SPECIFIC PATHOLOGY IMAGES WITH A MULTIMODAL CONDITIONED DIFFUSION MODEL FOR CELL AND NUCLEI SEGMENTATION

Dominik Winter*, Mai Bui*, Monica Azqueta Gavaldon*, Nicolas Triltsch*, Marco Rosati*, Nicolas Brieu*

* AstraZeneca Computational Pathology GmbH, Landsberger Str. 300, 80687 Munich, Germany

ABSTRACT

Scarcity of annotated data, particularly for rare or atypical morphologies, present significant challenges for cell and nuclei segmentation in computational pathology. While manual annotation is labor-intensive and costly, synthetic data offers a cost-effective alternative. We introduce a Multimodal Semantic Diffusion Model (MSDM) for generating realistic pixel-precise image-mask pairs for cell and nuclei segmentation. By conditioning the generative process with cellular/nuclear morphologies (using horizontal and vertical maps), RGB color characteristics, and BERT-encoded assay/indication metadata, MSDM generates datasests with desired morphological properties. These heterogeneous modalities are integrated via multi-head cross-attention, enabling fine-grained control over the generated images. Quantitative analysis demonstrates that synthetic images closely match real data, with low Wasserstein distances between embeddings of generated and real images under matching biological conditions. The incorporation of these synthetic samples, exemplified by columnar cells, significantly improves segmentation model accuracy on columnar cells. This strategy systematically enriches data sets, directly targeting model deficiencies. We highlight the effectiveness of multimodal diffusion-based augmentation for advancing the robustness and generalizability of cell and nuclei segmentation models. Thereby, we pave the way for broader application of generative models in computational pathology.

Index Terms— Diffusion models, Computational Pathology, Cell segmentation

1. INTRODUCTION

High-quality datasets, traditionally requiring labor-intensive and costly expert annotations [1], are crucial for deep learning in computational pathology, particularly for fundamental tasks like cell and nuclei segmentation upon which diagnosis, prognosis, and biomarker discovery are often based. While specialized methods such as Cellpose [2] generally deliver convincing results, their performance on specific morphologies, particularly rare ones, often suffers from a lack of high-quality training data. Synthetic data offers an efficient, cost-effective alternative to create realistic high-fidelity datasets [3]. In this study, we introduce MSDM, a Multimodal Semantic Diffusion Model, for generating synthetic immunohistochemistry (IHC) images. MSDM's strong conditioning capabilities enable the generation of data with desired morphological properties, directly addressing deficiencies in existing segmentation models for challenging morphologies or morphologies with low prevalence. Our goal is to generate realistic, pixel-precise image-mask pairs by re-using existing cell and nuclei annotations, ensuring the realism of the generated images. Unlike natural images with distinct objects, pathological images contain numerous, small, often touching cell instances requiring fine-grained spatial conditioning, aspects not fully

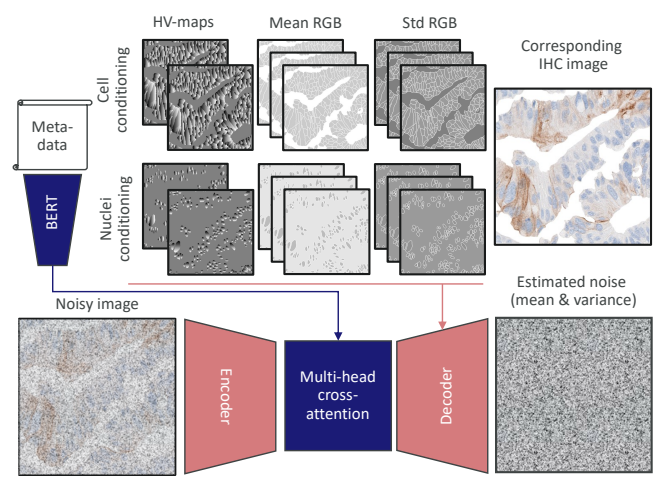


Fig. 1. MSDM overview: We condition the model on cell and nuclei morphologies using horizontal and vertical (HV) maps, and on RGB color characteristics (distinguishing foreground/background pixels). Additionally, BERT-encoded textual information conditions the diffusion model via a multi-head cross-attention mechanism to generate synthetic images that match the morphology of existing segmentation masks, creating a new image-mask pair for model training.

addressed by previous methods for this domain [4, 5]. We showcase our approach's capabilities to improve segmentation models' performance on low prevalence morphologies, exemplified on columnar cells. Columnar cells, characterized by large eccentricity (as defined in section 4.3), are underrepresented in our initial training dataset, leading to suboptimal performance of the segmentation model in our test set. Adding images of columnar cells generated with MSDM boosts the performance of segmentation models.

2. BACKGROUND

Synthetic data offers a cost-effective alternative to labor-intensive expert annotations. Early image-to-image translation (I2I) models, such as Pix2Pix, relied on CNNs and adversarial training to transfer images between domains while preserving content. These approaches have been successfully adapted in computational pathology for domain translation [6] and training data generation [7], enabling the reuse of existing annotations. Denoising diffusion probabilistic models (DDPMs), pioneered by Ho et al. [8], represent a significant advancement in generative modeling, demonstrating superior sample quality compared to GANs for both unconditional image generation and image-to-image tasks [9, 10, 11]. In computational pathology, DDPMs have enabled the generation of high-fidelity synthetic images across various applications, including

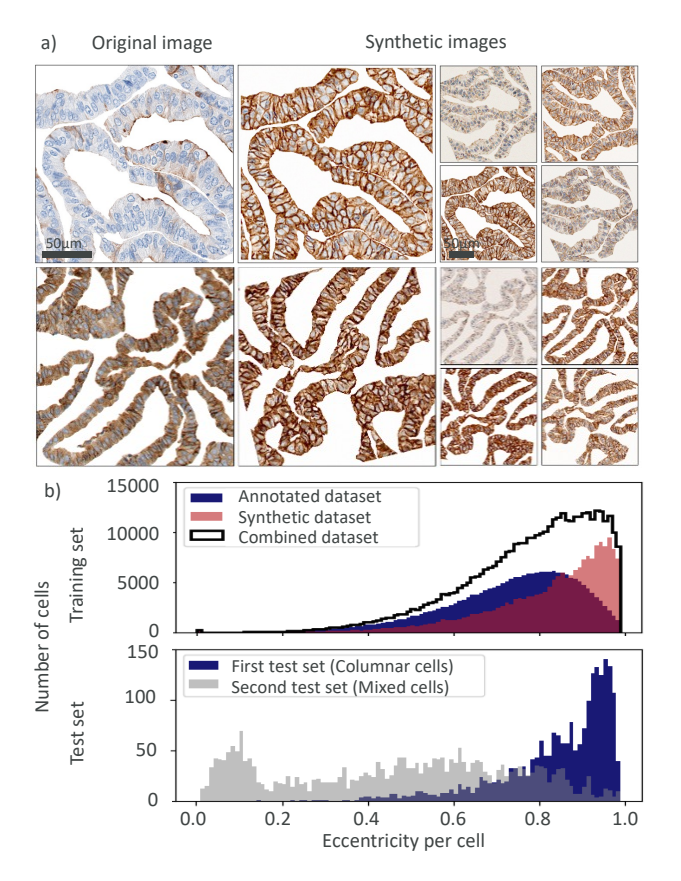


Fig. 2. a Original and corresponding synthetic images, for visualization images with the same (rotated) target mask are shown **b** Distribution of cell eccentricities in the training-set before and after data augmentation with MSDM and in the two test-sets.

H&E images, rare cancer datasets, and gigapixel pathology images [12, 13, 14, 15, 16, 17, 18, 19, 20]. The introduction of conditional DDPMs enabled targeted data generation by constraining the inherently stochastic diffusion process through various guidance mechanisms [21]. Building upon conditional DDPMs, semantically conditioned diffusion models (SDMs) [4] have advanced guided medical image generation, particularly in brain MRI [22] and H&E image synthesis [5]. These models leverage high-level contextual cues through semantic label maps for targeted synthesis of anatomical structures. The SDM architecture employs a U-Net-based conditional denoising network that processes noisy images through encoder blocks while injecting semantic label maps into decoder blocks via spatially-adaptive normalization (SPADE) [23]. The encoder incorporates timestep-dependent scaling through specialized residual blocks, while the decoder uses SPADE to enable spatiallyadaptive feature modulation. Parallel to semantic conditioning, textconditioned diffusion models guide synthesis using natural language prompts [24], finding applications in biomedical image generation for H&E slides [25] and spatially consistent nuclei generation [26]. However, applying conventional SDMs to computational pathology presents unique challenges. Addressing pathology-specific challenges, namely that pathological images contain numerous, small, often touching cell instances, necessitates more fine-grained spatial conditioning for enhanced instance separation, which conventional semantic conditioning approaches do not fully address. Our work extends these conditioning mechanisms by integrating multimodal

guidance to meet the specific requirements of pathological image synthesis.

3. METHODS

3.1. MSDM: Extending the semantic diffusion model

We re-implemented the SDM [4] based on the guided diffusion model [9] to meet the requirements of computational pathology by first adapting the semantic maps that guide the diffusion process to horizontal and vertical (HV) maps. These HV maps are calculated as the horizontal/vertical distances to the boundaries of each instance (e.g., cell/nuclei boundaries), enhancing instance separation. We extend the conditioning with RGB color characteristics, creating a 16-channel guidance maps. For both cells and nuclei, we include HV maps (2 channels), mean RGB values (3 channels), and RGB standard deviations (3 channels), totaling 8 channels for cells and eight channels for nuclei. These maps display one constant value for the mean and standard deviation of all cells and for the mean and standard deviation of all nuclei in a given image. This 16-channel mask guides the diffusion process via SPADE normalization in the U-Net decoder (see figure 1) [23]. To further enhance guidance, we add text conditioning using BERT-tiny [27] to encode assay and indication information. Multi-head cross-attention in the diffusion model's U-Net bottleneck fuses encoder features with text tokens. The bottleneck was chosen for its semantically rich image representation, maximal global context, and computational efficiency due to the most feature compression.

3.2. Multimodal feature fusion

Multimodal feature fusion employs multi-head cross-attention, integrating image and text features for semantically and textually guided image generation. The latent representations of the current noisy image (image features) and the encoded text embeddings are fused using cross-attention. Given the image feature matrix $(X \in \mathbb{R}^{H \times W \times C})$ and the text feature matrix $(T \in \mathbb{R}^{L \times D})$, the model projects these to query, key, and value spaces as follows: $Q = XW_Q$, $K = TW_K$, $V = TW_V$ where (W_Q, W_K) , and W_V) are learnable projection matrices. For each attention head, the cross-attention is computed as:

$$Attention(Q, K, V) = softmax \left(\frac{QK^T}{\sqrt{d}}\right)V$$
 (1)

Here, queries come from image features and keys/values from text, allowing the model to align and integrate textual context at each spatial location. We run eight attention heads $i \in \{0, \dots, 7\}$ in parallel, each capturing different image–text correlation patterns.

$$\begin{aligned} & \text{MultiHeadAttention}(Q, K, V) = \\ & \left(\text{Concat}_{i=1}^{h} \left(\text{Attention}(Q_i, K_i, V_i) \right) \times W^O \right) + b^o \end{aligned} \tag{2}$$

The attended feature vector is added to the image feature vector. This fused representation is propagated through the diffusion denoising steps, allowing the model to iteratively refine image predictions in a way that accurately reflects the provided textual guidance.

Latent space features were investigated by embedding real and synthetic images using the H-Optimus-0 foundation model [28], visualizing embeddings with UMAP [29], and calculating Wasserstein distances [30] between distributions.

4. EXPERIMENTS

We compare the baseline Semantic Diffusion Model (SDM), only modified with 4-channel HV spatial conditioning for cell and nuclei specificity with our MSDM.

4.1. Model training

Both diffusion models for data augmentation were trained using the ADAM optimizer with mean squared error loss and a cosine noise scheduler for 20,000 epochs. A batch size of 5 with 5 gradient accumulation steps yielded an effective batch size of 25. During inference, we used DDIM scheduler [10] with 40 timestep respacing steps, yielding 25-fold faster inference versus DDPM scheduler. The validation set remained constant for all trainings.

4.2. Datasets

Our training dataset comprises 566 immunohistochemistry (IHC)stained slides (e.g., HER2 membrane marker assay, 20x magnification). From these, 612 Field-of-Views (FOVs) of size 512x512 pixels were selected. A group of board-certified pathologists annotated all cell and nuclei outlines within the tumor epithelium of these FOVs, yielding 307,666 cell and 232,031 nuclei outlines for the training set. The manually annotated validation dataset was established using 267 independent IHC-stained slides, also featuring the same assay. A total of 309 FOVs of size 512x512 pixels were selected from these slides, and all cell and nuclei outlines within them were annotated by a single pathologist. This resulted in 153,873 annotated cell outlines and 110,834 annotated nuclei outlines. We have two test sets, the first containing mainly columnar cells and the second containing a mix of indications and cells. Our first test set contains 36 FOVs (512×512 pixel) from 29 IHC slides; the second has 303 FOVs from 147 slides representing diverse indications and assays, with no particular focus on columnar cells. Within the tumor epithelium, cell centers were independently annotated by three pathologists for all FOVs, and cell/nuclei outlines for selected cells. First test set annotation counts (P1/P2/P3): cell centers—12869/12741/14186; cell outlines—933/698/698; nuclei outlines—898/699/698. Second test set: cell centers—196825/12741/14186; cell outlines—149074/5672/6177; nuclei outlines—155560/5668/6219. Only tumor epithelium regions were annotated and analyzed.

4.3. Dataset enhancement with the diffusion model

To focus our augmentation efforts on columnar cells, we identified FOVs in our training dataset containing cells with high eccentricity. Cell eccentricity was calculated by fitting an ellipse to the cell shape and determining its eccentricity e from the minor/major axes ratio:

$$e = \sqrt{1 - \left(\frac{L_{\text{minor}}}{L_{\text{major}}}\right)^2} \tag{3}$$

FOVs with an average cell eccentricity e>0.85 were chosen, yielding 120 FOVs (of the 612 FOVs in the training dataset). For image generation, one cell mask was randomly chosen from the 120 chosen FOVs, together with its corresponding nuclei mask. Color and metadata conditions were randomly selected from the 120 chosen FOVs. Choosing newly matched condition pairs for each image generation, we generated eight new versions for each FOV, resulting in 960 synthetic FOVs (see figure 2). Re-using existing masks, color,

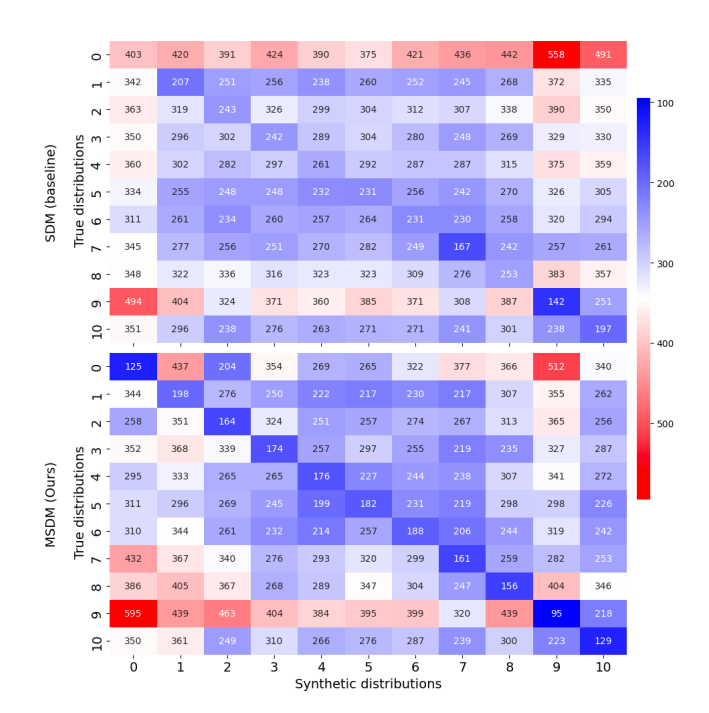


Fig. 3. Wasserstein distances in latent space embeddings between real (y-axis) and synthetic (x-axis) images corresponding to different combination of assay and indication pairs (e.g. 1:=HER2/Breast,...). Matching pairs lie on the diagnonal of the so-formed matrices.

and metadata ensured synthetic images were realistic examples, reflecting desired morphological properties.

4.4. Evaluation

To assess the impact of our synthetic data in downstream segmentation tasks, Cellpose [2] models were trained for cell and nuclei segmentation under three distinct scenarios, all utilizing the same validation set for consistent evaluation. These scenarios include: (1) training with all 612 annotated real training data only (serving as our baseline); (2) training with all 612 annotated real training data plus 960 synthetic images created with the SDM model; and (3) training with all 612 annotated real training data plus 960 synthetic images created with our MSDM model. The synthetic data generated by SDM and MSDM was combined with existing imagemask pairs in the training dataset (see figure 2). The segmentation models were benchmarked against three pathologists' annotations on the test set using F1 score for cell center detection, average symmetric surface distance (ASSD) for membrane segmentation, and Dice score for cytoplasm and nuclei segmentation (after Hungarian matching). We prioritized cell center detection (F1 score) for evaluating performance because other metrics (membrane, cytoplasm, nuclei segmentation) are dependent on successful cell center identification via Hungarian matching. For final results (see Table 1), each model training was repeated five times, evaluated against all three pathologists, and metrics were averaged. To statistically assess the significance of observed differences in performance between models, we employed a Wilcoxon signed-rank test, considering a difference significant when the p-value was less than p < 0.05. Beyond assessing the utility of synthetic data for downstream tasks, we evaluated the faithfulness of the synthetic data. Therefore, we calculated the Wasserstein distances in latent space embeddings between

indication-assay pairs of real and synthetic data contained in the validation set (see Figure 3). This approach provides insight into how closely the embedding space of the synthetic data aligns with that of the real data, thereby indicating how well the generative models capture the underlying data distribution.

5. RESULTS

MSDM demonstrates effectiveness through two key evaluations. First, we verify conditioning efficacy by generating images guided by textual inputs (indications and assays). Using metadata, we identified ten distinct indication-assay pairs as clusters for evaluating conditioning. We used H-Optimus-0, a state-of-the-art computational pathology foundation model, to embed synthetic images generated from these pairs and corresponding real validation images. In the embedding space, we computed Wasserstein distances between real and synthetic data for each of the ten indication-assay pairs. MSDM achieved significantly lower average Wasserstein distances (158.75 \pm 29.50; $mean \pm sdev$) for matching distributions and for for non-matching distributions (303.46 \pm 69.73) (see Fig. 3) than the SDM model (matching: 234.18 ± 63.92 ; non-matching: 312.87 ± 61.95). Second, we investigated performance improvements in columnar cell and nuclei segmentation using our synthetic data. MSDM yielded best results (see Table 1), significantly outperforming models trained solely on real data and surpassing the SDM model. On our second test set containing mixed cells, our approach increases cytoplasm and nuclei segmentation performance while retaining cell center detection and membrane segmentation performance.

First test set (Columnar cells)				
Results	Cell cen-	Membrane	Cytoplasm	Nuclei
	ter detec-	segmenta-	segmenta-	segmenta-
	tion	tion	tion	tion
Metric	F1 [%]	ASSD	Dice score [%]	
	↑ better	↓ better	↑ better	
IPA	86.62±0.82	0.62 ± 0.02	72.18±1.42	90.32 ± 0.63
Baseline	81.99±0.77	0.99 ± 0.04	63.68±1.37	81.52±1.29
SDM	81.64±0.74	0.97 ± 0.04	64.36±1.39	82.14±1.35
	*	*	*	*
MSDM	82.30±0.87	$0.96 {\pm} 0.04$	64.19±1.47	82.23±1.37
	*×	*	*	*
Second test set (Mixed cells)				
IPA	86.49	0.70	71.09	90.27
Baseline	83.75	1.03	62.92	84.53
MSDM	83.75	1.03	64.31 *	85.31 *

Table 1. Reported values are means (std $< 10^{-5}$ unless stated). IPA: agreement among three pathologists. Significant differences (p < 0.05): \star (baseline vs. SDM/MSDM), \times (SDM vs. MSDM).

6. DISCUSSION

In this study, we modified a semantic diffusion model, creating a novel multimodal-conditioned generative framework for computational pathology. Our architectural enhancements, incorporating HV maps for morphology, RGB color, and BERT-encoded metadata, enable the generation of targeted synthetic data to specifically enhance the segmentation performance of morphologies with low prevalence, exemplified on columnar cells. The observed Wasserstein distances

between embedded real and synthetic data for matching biological conditions demonstrate our model's capacity to faithfully capture crucial morphological and contextual nuances, as compared to the SDM. In a downstream application, the synthetically generated images significantly boost the performance of cell and nuclei segmentation models on IHC-stained images, yielding superior performance as compared to models trained on real data alone or data generated with the SDM model. In comparison to manually annotating FOVs by a pathologists, which we estimate to take around 4 hours per FOV (accumulating to 3840 hours for 960 FOVs) this presents a significant time and cost saving, although one might argue that FOVs placed and annotated by pathologists might be of larger benefit for model training. We acknowledge that, by reusing existing masks, our current approach for synthetic data generation requires an initial set of annotations on cells with challenging morphologies. This implies that while our method effectively augments existing datasets, it does not fully circumvent the need for initial annotations. In future work, we plan to explore broader applications, including other challenging morphologies, diverse assays, and potential computational efficiencies, to fully leverage the power of multimodal diffusion models for data augmentation in computational pathology. This study thus underscores the potential of generative models in overcoming data scarcity and advancing model robustness for critical pathology tasks.

7. COMPLIANCE WITH ETHICAL STANDARDS

The study was conducted in adherence to the International Council for Harmonization Good Clinical Practice guidelines, the Declaration of Helsinki, and local regulations on the conduct of clinical research. The AstraZeneca Biobank in the UK is licensed by the Human Tissue Authority (License No. 12109) and has National Research Ethics Service Committee (NREC) approval as a Research Tissue Bank (RTB) (REC No 17/NW/0207) which covers the use of the samples for this project. The studies were conducted in accordance with the local legislation and institutional requirements. The participants provided their written informed consent to participate in this study.

8. ACKNOWLEDGMENTS

All authors are employees of AstraZeneca and do not have other relevant financial or non-financial interests to disclose. We thank Helen Angell, Mari Heininen-Brown, and Andrea Storti on behalf of the Tumour & Immune Cell Atlas team (TICA, AstraZeneca), whose end-to-end stewardship of a large, rigorously curated histological slide database (sourcing, staining, digitalisation, curation and QA) enabled the training of our diffusion models.

9. REFERENCES

- [1] Jeroen Van der Laak, Geert Litjens, and Francesco Ciompi, "Deep learning in histopathology: the path to the clinic," *Nature medicine*, vol. 27, no. 5, pp. 775–784, 2021.
- [2] Carsen Stringer, Tim Wang, Michalis Michaelos, and Marius Pachitariu, "Cellpose: a generalist algorithm for cellular segmentation," *Nature methods*, vol. 18, no. 1, pp. 100–106, 2021.
- [3] Amirhossein Kazerouni, Ehsan Khodapanah Aghdam, Moein Heidari, Reza Azad, Mohsen Fayyaz, Ilker Hacihaliloglu, and Dorit Merhof, "Diffusion models in medical imaging: A comprehensive survey," *Medical Image Analysis*, p. 102846, 2023.

- [4] Weilun Wang, Jianmin Bao, Wengang Zhou, Dongdong Chen, Dong Chen, Lu Yuan, and Houqiang Li, "Semantic image synthesis via diffusion models," arXiv preprint arXiv:2207.00050, 2022.
- [5] Meilong Xu, Saumya Gupta, Xiaoling Hu, Chen Li, Shahira Abousamra, Dimitris Samaras, Prateek Prasanna, and Chao Chen, "Topocellgen: Generating histopathology cell topology with a diffusion model," in *Proceedings of the Computer Vision* and Pattern Recognition Conference, 2025, pp. 20979–20989.
- [6] Nicolas Brieu, Nicolas Triltsch, Philipp Wortmann, Dominik Winter, Shashank Saran, Marlon Rebelatto, and Günter Schmidt, "Auxiliary cyclegan-guidance for task-aware domain translation from duplex to monoplex ihc images," arXiv:2403.07389, 2024.
- [7] Dominik Winter, Nicolas Triltsch, Philipp Plewa, Marco Rosati, Thomas Padel, Ross Hill, Markus Schick, and Nicolas Brieu, "Restaingan: Leveraging ihc to if stain domain translation for in-silico data generation," arXiv:2403.06545, 2024.
- [8] Jonathan Ho, Ajay Jain, and Pieter Abbeel, "Denoising diffusion probabilistic models," *Advances in neural information* processing systems, vol. 33, pp. 6840–6851, 2020.
- [9] Prafulla Dhariwal and Alexander Nichol, "Diffusion models beat gans on image synthesis," *Advances in neural information processing systems*, vol. 34, pp. 8780–8794, 2021.
- [10] Jiaming Song, Chenlin Meng, and Stefano Ermon, "Denoising diffusion implicit models," *arXiv:2010.02502*, 2020.
- [11] Alexander Quinn Nichol and Prafulla Dhariwal, "Improved denoising diffusion probabilistic models," in *International conference on machine learning*. PMLR, 2021, pp. 8162–8171.
- [12] Puria Azadi Moghadam, Sanne Van Dalen, Karina C Martin, Jochen Lennerz, Stephen Yip, Hossein Farahani, and Ali Bashashati, "A morphology focused diffusion probabilistic model for synthesis of histopathology images," in *Proceedings of the IEEE/CVF winter conference on applications of computer vision*, 2023, pp. 2000–2009.
- [13] Hyun-Jic Oh and Won-Ki Jeong, "Diffmix: Diffusion model-based data synthesis for nuclei segmentation and classification in imbalanced pathology image datasets," in *International Conference on Medical Image Computing and Computer-Assisted Intervention*. Springer, 2023, pp. 337–345.
- [14] Aman Shrivastava and P Thomas Fletcher, "Nasdm: nuclei-aware semantic histopathology image generation using diffusion models," in *International Conference on Medical Image Computing and Computer-Assisted Intervention*. Springer, 2023, pp. 786–796.
- [15] Tushar Kataria, Beatrice Knudsen, and Shireen Y Elhabian, "Staindiffuser: Multitask dual diffusion model for virtual staining," arXiv:2403.11340, 2024.
- [16] Xinyi Yu, Guanbin Li, Wei Lou, Siqi Liu, Xiang Wan, Yan Chen, and Haofeng Li, "Diffusion-based data augmentation for nuclei image segmentation," in *International Conference on Medical Image Computing and Computer-Assisted Intervention*. Springer, 2023, pp. 592–602.
- [17] Srikar Yellapragada, Alexandros Graikos, Prateek Prasanna, Tahsin Kurc, Joel Saltz, and Dimitris Samaras, "Pathldm: Text conditioned latent diffusion model for histopathology," in *Pro*ceedings of the IEEE/CVF Winter Conference on Applications of Computer Vision, 2024, pp. 5182–5191.

- [18] Robert Harb, Thomas Pock, and Heimo Müller, "Diffusion-based generation of histopathological whole slide images at a gigapixel scale," in *Proceedings of the IEEE/CVF Winter Conference on Applications of Computer Vision*, 2024, pp. 5131–5140
- [19] Marco Aversa, Gabriel Nobis, Miriam Hägele, Kai Standvoss, et al., "Diffinfinite: Large mask-image synthesis via parallel random patch diffusion in histopathology," *Advances in Neural Information Processing Systems*, vol. 36, 2024.
- [20] Dominik Winter, Nicolas Triltsch, Marco Rosati, Anatoliy Shumilov, Ziya Kokaragac, Yuri Popov, Thomas Padel, Laura Sebastian Monasor, Ross Hill, Markus Schick, et al., "Utilizing mask-guided cross-image attention for zero-shot in-silico histopathologic image generation with a diffusion model," in 2025 IEEE 22nd International Symposium on Biomedical Imaging (ISBI). IEEE, 2025, pp. 1–5.
- [21] Alex Nichol, Prafulla Dhariwal, Aditya Ramesh, Pranav Shyam, Pamela Mishkin, Bob McGrew, Ilya Sutskever, and Mark Chen, "Glide: Towards photorealistic image generation and editing with text-guided diffusion models," *arXiv* preprint arXiv:2112.10741, 2021.
- [22] Alex Ling Yu Hung, Kai Zhao, Haoxin Zheng, Ran Yan, Steven S Raman, Demetri Terzopoulos, and Kyunghyun Sung, "Med-cdiff: conditional medical image generation with diffusion models," *Bioengineering*, vol. 10, no. 11, pp. 1258, 2023.
- [23] Taesung Park, Ming-Yu Liu, Ting-Chun Wang, and Jun-Yan Zhu, "Semantic image synthesis with spatially-adaptive normalization," in *Proceedings of the IEEE/CVF conference on* computer vision and pattern recognition, 2019, pp. 2337– 2346.
- [24] Omri Avrahami, Dani Lischinski, and Ohad Fried, "Blended diffusion for text-driven editing of natural images," in Proceedings of the IEEE/CVF conference on computer vision and pattern recognition, 2022, pp. 18208–18218.
- [25] Aakash Madhav Rao and Debayan Gupta, "Improving text-conditioned latent diffusion for cancer pathology," arXiv preprint arXiv:2412.06487, 2024.
- [26] Hyun-Jic Oh and Won-Ki Jeong, "Controllable and efficient multi-class pathology nuclei data augmentation using textconditioned diffusion models," in *International Conference* on Medical Image Computing and Computer-Assisted Intervention. Springer, 2024, pp. 36–46.
- [27] Jacob Devlin, Ming-Wei Chang, Kenton Lee, and Kristina Toutanova, "Bert: Pre-training of deep bidirectional transformers for language understanding," in *Proceedings of the 2019 conference of the North American chapter of the association for computational linguistics: human language technologies, volume 1 (long and short papers)*, 2019, pp. 4171–4186.
- [28] C. Saillard et al., "H-optimus-0," https://github.com/bioptimus, 2024, GitHub.
- [29] Leland McInnes, John Healy, and James Melville, "Umap: Uniform manifold approximation and projection for dimension reduction," arXiv:1802.03426, 2018.
- [30] Leonid Nisonovich Vaserstein, "Markov processes over denumerable products of spaces, describing large systems of automata," *Problemy Peredachi Informatsii*, vol. 5, no. 3, pp. 64–72, 1969.